High-Isolation In-Band Full-Duplex Cavity-Backed Slot Antennas in a Single Resonant Cavity

Rui-Sen Chen, *Graduate Student Member, IEEE*, Lei Zhu, *Fellow, IEEE*, Jing-Yu Lin, *Graduate Student Member, IEEE*, Sai-Wai Wong, *Senior Member, IEEE*, Yang Yang, *Senior Member, IEEE,* Yin Li, *Member, IEEE,* Long Zhang, *Member, IEEE,* and Yejun He, *Senior Member, IEEE*

***Abstract*— High-isolation in-band full-duplex (IBFD) cavity-backed slot antennas (CBSAs) in a single resonant cavity are presented in this article. The TE_{101} and TE_{011} cavity modes combined with a modified orthogonal feeding structure are first used to design the duplex antenna. The proposed feeding structure can reduce the port-to-port coupling strength and produce a very high isolation. By replacing the crossed radiation slots with two pairs of parallel radiation slots, enhanced radiation gain is achieved. To tackle the narrow bandwidth for the single-mode operation, two orthogonal resonant-iris modes produced by the two feeding slots are introduced to design a dual-mode wideband IBFD antenna. The simulated bandwidth is increased from 0.8% to 5.7%. All the presented antennas with improved performances are designed and realized in a single full-metal resonant cavity. Compared with the conventional design method, high isolation, enhanced gain, and enhanced bandwidth are simultaneously achieved without enlarging the antenna size. Finally, the prototype of the wideband IBFD slot antenna is measured and presented to validate the design concept, which has a 5.8% bandwidth, higher than 95% total efficiency, especially an isolation higher than 72 dB.**

***Index Terms*— Cavity-backed slot antenna (CBSA), enhanced bandwidth, enhanced gain, full metal, high isolation, in-band full-duplex (IBFD).**

Manuscript received July 10, 2020; revised September 17, 2020; accepted October 7, 2020. Date of publication October 27, 2020; date of current version October 28, 2021. This work was supported in part by the Shenzhen Science and Technology Program under Grant JCYJ20180305124543176 and Grant JCYJ20190728151457763; in part by the Natural Science Foundation of Guangdong Province under Grant 2018A030313481; in part by the Shenzhen University Research Startup Project of New Staff under Grant 860-000002110311; and in part by the National Natural Science Foundation of China under Grant 62071306. *(Corresponding authors: Sai-Wai Wong; Yejun He.)*

Rui-Sen Chen is with the College of Electronics and Information Engineering, Shenzhen University, Shenzhen 518060, China, and also with the Department of Electrical and Computer Engineering, Faculty of Science and Technology, University of Macau, Macau 999078, China.

Lei Zhu is with the Department of Electrical and Computer Engineering, Faculty of Science and Technology, University of Macau, Macau 999078, China.

Jing-Yu Lin and Yang Yang are with the School of Electrical and Data Engineering, University of Technology Sydney, Ultimo, NSW 2007, Australia.

Sai-Wai Wong, Yin Li, Long Zhang, and Yejun He are with the College of Electronics and Information Engineering, Shenzhen University, Shenzhen 518060, China (e-mail: wongsaiwai@ieee.org; heyejun@126.com).

Color versions of one or more of the figures in this article are available online at https://ieeexplore.ieee.org.

Digital Object Identifier 10.1109/TAP.2020.3032846

I. Introduction

IN-BAND full-duplex(IBFD) systems, also known as simultaneous transmit and receive (STAR) systems, can improve the spectral efficiency to resolve the congested frequency spectrum of the modern wireless systems. The main challenge in the implementation of the IBFD systems is the high self-interference (SI) cancellation (>100 dB) between transmitting channels (Tx) and receiving channel (Rx). The fulfillment of the high SI cancellation can be realized with the combination of several factors: 1) antenna design; 2) analog cancellation; and 3) digital cancellation.

In this work, we focus on the design of the IBFD antenna. High-isolation IBFD antennas have been attracting much attention as they can degrade the signal from the Tx to Rx and also alleviate the requirements of analog and digital SI cancellation. The approaches of designing high-isolation IBFD antennas include the dual-antenna structure and single-antenna structure. The first approach is using separate antenna elements for Tx and Rx channels [1]–[4]. In [1], a spatial duplexing filter and two separate antennas with orthogonal polarizations were used to reduce the Tx–Rx coupling. In [2] and [3], two orthogonal linearly polarized antennas with an auxiliary port for the decoupling were used to improve the SI cancellation and achieved an isolation of 40 dB. This approach usually requires a large physical distance and does not satisfy the desired form of modern wireless systems. While the IBFD antennas designed on a single antenna have a compact size and are much attractive in the IBFD systems, as discussed in [5], several practical design methods of the orthogonal-polarized single-antenna IBFD antennas have been reported in the literature [6]–[14]. In [6] and [7], the horizontal polarization and vertical polarization of a single patch antenna are used to achieve the high isolation of the IBFD antenna. Besides, differential feeding of one port [8]–[12] or both two ports [13], [14] of the patch antennas were introduced to improve the SI cancellation. In [13], each port is fed with a 3 dB/180° ring coupler to form a double-differential feeding patch antenna, which can achieve an isolation of 72 dB over the operating band.

The aforementioned IBFD antennas were designed on microstrip-line structure, which had a small size and low

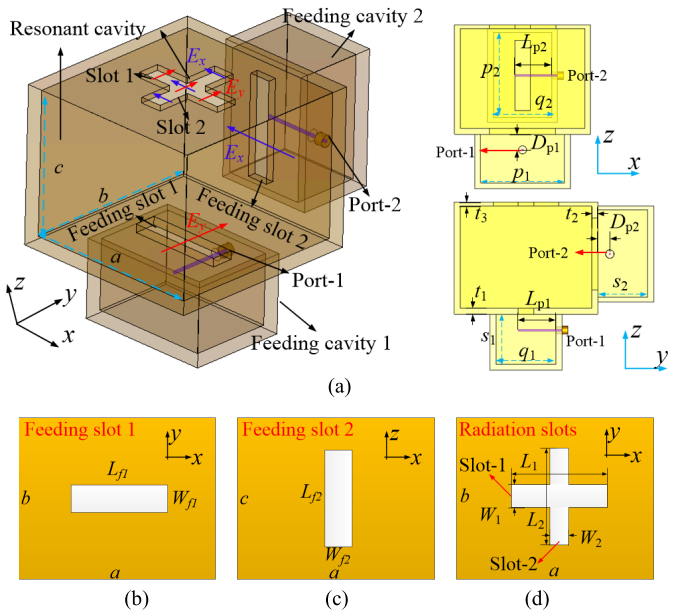

Fig. 1. Proposed duplex CBSA. (a) 3-D view. (b) View of feeding slot 1. (c) View of feeding slot 2. (d) View of radiation slots.

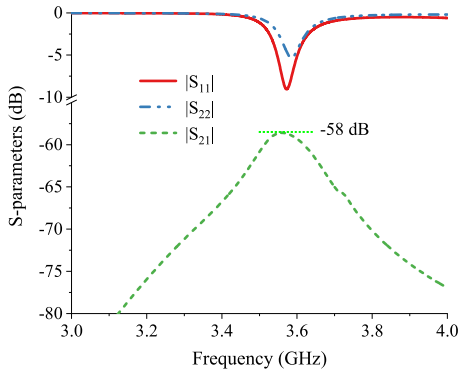

Fig. 2. Initial performance of the duplex antenna. Dimensions (unit: mm): $a = b = 66$, $c = 50$, $p_1 = p_2 = 44$, $q_1 = q_2 = 30$, $s_1 = s_2 = 25$, $L_1 = L_2 = 34$, $W_1 = W_2 = 7$, $L_{f1} = L_{f2} = 32$, $W_{f1} = W_{f2} = 4$, $L_{p1} = L_{p2} = 16$, $D_{p1} = D_{p2} = 6$, $t_1 = t_2 = 3$, and $t_3 = 2$.

cost while suffering from low gain and low efficiency. Cavity-backed slot structure [15]–[22] can tackle these challenges, and it is a good candidate to design high-gain and high-efficiency antennas. Especially, the full-metal cavity-backed slot antennas (CBSAs) [19]–[22] have high-power-handling capacity and are highly demanded for the long-range and high-power wireless systems. SIW IBFD CBSA [23], [24] and full-metal IBFD CBSAs [25], [26] based on orthogonal polarizations were reported to achieve high gain and high efficiency. In [24], a double-differential-fed IBFD SIW cavity slot antenna using TE_{120} and TE_{210} modes is reported, which can obtain a high isolation of 60 dB. In [25], two separate corporate-feeding networks in different layers of the feeding network for the two different polarizations were used to feed the slot antenna and achieved an isolation of 52 dB.

In this article, a class of full-metal IBFD CBSAs with high isolation are presented. All the antennas are implemented on a single resonant cavity. Two orthogonal rectangular-waveguide cavity modes, i.e., TE_{101} and TE_{011}, combined with a modified orthogonal feeding structure, are first used to design the dual-polarized duplex antenna. Then, the detailed analysis of the improved isolation produced by the proposed arrangement of the feeding structures, as shown in Fig. 1(a), is presented. This configuration can reduce the port-to-port coupling strength and obtain a much higher isolation than the conventional one [19]. Besides, by replacing the two crossed radiation slots with two pairs of parallel radiation slots, an enhanced gain is achieved. Furthermore, additional orthogonal resonant-iris modes [27] produced by the feeding slots are combined with the cavity modes to design a dual-mode duplex antenna with enhanced bandwidth. The operating bandwidth is increased from 0.8% to 5.7%. All the improvements of high isolation, enhanced gain, and enhanced bandwidth are achieved without introducing extra structure, enlarging cavity size, or deteriorating other antenna's performances. Finally, the enhanced-bandwidth and enhanced-gain IBFD slot antenna is fabricated and measured. Measurement shows that the antenna can achieve a 5.8% bandwidth at 3.47 GHz, and the port-to-port isolation is higher than 72 dB over the operating band.

II. Basic Operating Principle

A. Proposed In-Band Full-Duplex Slot Antenna

Fig. 1 shows the physical structure of the proposed duplex CBSA. It is composed of a resonant cavity with two feeding slots and a pair of crossed slots, two coaxial-to waveguide transitions formed by the feeding cavity, and the SMA port with the extended probe. The coaxial-to-waveguide transitions are used to excite the cavity modes via the feeding slots. In this antenna, the two cavity modes, TE_{101} and TE_{011}, which have orthogonal electric field distributions, are first used to achieve the duplex performance.

Feeding slots 1 and 2 are used to excite the cavity modes TE_{101} and TE_{011}, respectively, whereas radiation slots 1 and 2 are used to radiate the energy of TE_{101} and TE_{011}, respectively. The orthogonal field distributions of these two modes inherently ensure good isolation.

Fig. 2 shows an initial performance of the proposed duplex antenna. The initial size of the antenna is given in Fig. 2, and the dimensions related to channels 1 and 2 are set identical to show the initial performance and to easily carry out the subsequent analysis. It can be seen that there is a difference in the operating frequency between these two channels, which is due to that the feeding structures of them are not exactly the same, i.e., the positions of the feeding structures with the reference of the radiation slots. The isolation between the two channels attains about 58 dB. Thus, the proposed antenna holds good duplex property as desired.

Here, the adjustment of the resonant frequencies of the two channels is first presented and analyzed. To deal with this issue, the equivalent circuit models of the duplex antenna are provided, as shown in Fig. 3. Each channel is expressed as an individual circuit model. The cavity modes can be seen as a parallel *LC* resonator, and both the feeding slot and radiation slot produce a shunt capacitive loading on the cavity modes.

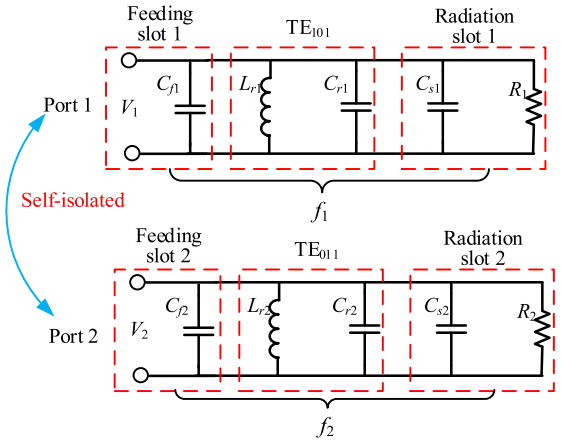

Fig. 3. Equivalent circuit model of the proposed duplex antenna.

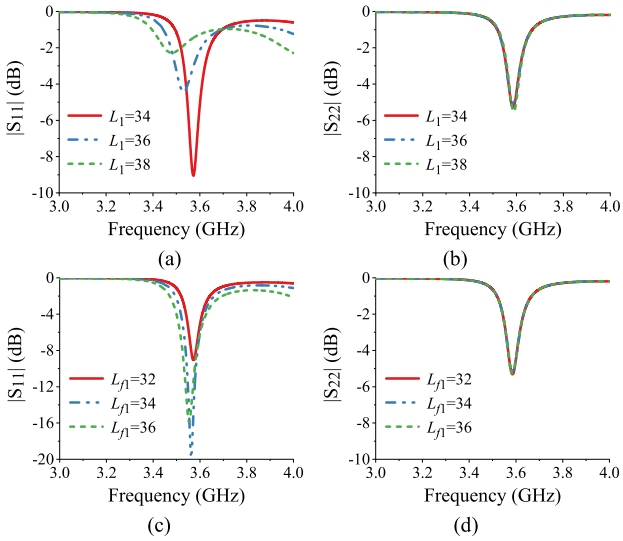

Fig. 4. Effect of the lengths of slot 1 and feeding slot 1 on f_1 and f_2. (a) and (b) Versus L_1. (c) and (d) Versus L_{f1}. Dimensional unit: mm.

According to Fig. 3, the resonant frequencies of the two cavity modes under the effect of the loaded slots, i.e., f_1 and f_2, are calculated as (1) and (2), respectively. It can be seen that f_1 can be individually adjusted by modifying C_{f1} and C_{s1}, i.e., by modifying the sizes of the feeding slot 1 and radiation slot 1 and f_2 can be individually adjusted by modifying C_{f2} and C_{s2}, i.e., by modifying the sizes of the feeding slot 2 and radiation slot 2

$$f_1 = \frac{1}{2\pi\sqrt{L_{r1}(C_{r1}+C_{f1}+C_{s1})}} \tag{1}$$

$$f_2 = \frac{1}{2\pi\sqrt{L_{r2}(C_{r2}+C_{f2}+C_{s2})}}. \tag{2}$$

To prove this analysis, Fig. 4 shows the effects of the size of feeding slot 1 and radiation slot 1 on these two modes of f_1 and f_2. Fig. 4(a) shows that the increasing length of the radiation slot 1, i.e., L_1, introduces a decreasing frequency of f_1, as an increasing length of the slot produces an increasing loading capacitance C_{s1}. Meanwhile, the increasing L_1 does not affect f_2, as radiation slot 1 is parallel to the electric field

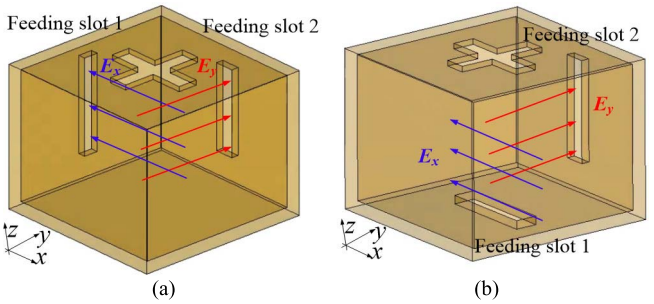

Fig. 5. Configurations of (a) conventional and (b) proposed duplex slot antennas. Feeding cavities and probes are not shown here.

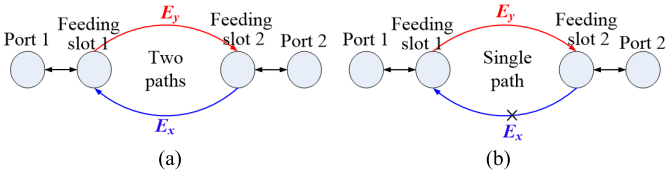

Fig. 6. Coupling topologies of (a) conventional and (b) proposed duplex slot antennas.

of f_2. Fig. 4(c) and (d) shows that an increasing length of feeding slot 1 also causes a decreasing f_1, while it does not affect f_2. Besides, the varying size of the radiation slot has a larger effect on the resonant frequency than the varying size of the feeding slot. Similarly, it can be predicted that the slots' length of radiation slot 2 and feeding slot 2 only affects f_2. Thus, both the frequencies of f_1 and f_2 can be individually controlled and can help to design the IBFD antenna.

B. Analysis of Improved Isolation

The isolation mainly depends on the coupling between the two ports. The high isolation of the proposed duplex antenna is obtained under a purposed arrangement of the two feeding structures, which can reduce the coupling between the two ports. For the comparison, the conventional IBFD antenna with a different arrangement of the feeding structures is presented. The configurations of these two duplex antennas are shown in Fig. 5 for comparative study. Here, only the feeding slots on behalf of the feeding structures are shown here. From Fig. 5(a), it can be seen that the electric field E_y produced by feeding slot 1 transmits toward feeding slot 2 and the electric field E_x produced by feeding slot 2 transmits toward feeding slot 1, which means that there are two coupling paths between the two ports. For the proposed duplex antenna shown in Fig. 5(b), the electric field E_y produced by feeding slot 1 transmits toward feeding slot 2, however, the electric field E_x produced by feeding slot 2 is parallel to feeding slot 1 and thus cannot transmit toward feeding slot 1, which means that there is only one coupling path between the two ports of the proposed duplex antenna. The coupling topologies of them are shown in Fig. 6(a) and (b). Thus, the proposed duplex slot antenna has a reduced coupling strength and can obtain a high isolation. The simulated isolation shown in Fig. 7 indicates that the conventional antenna can only achieve an in-band isolation of 18 dB, which is much lower than the proposed

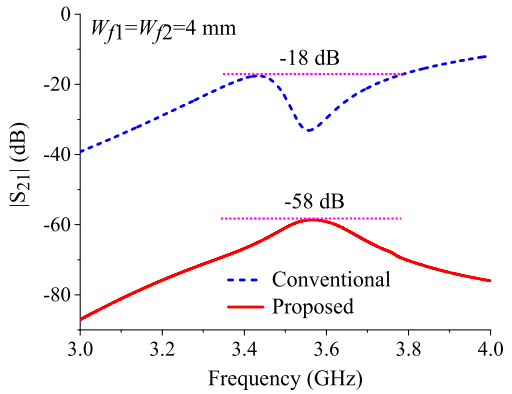

Fig. 7. Simulated isolations of the conventional and proposed duplex slot antennas.

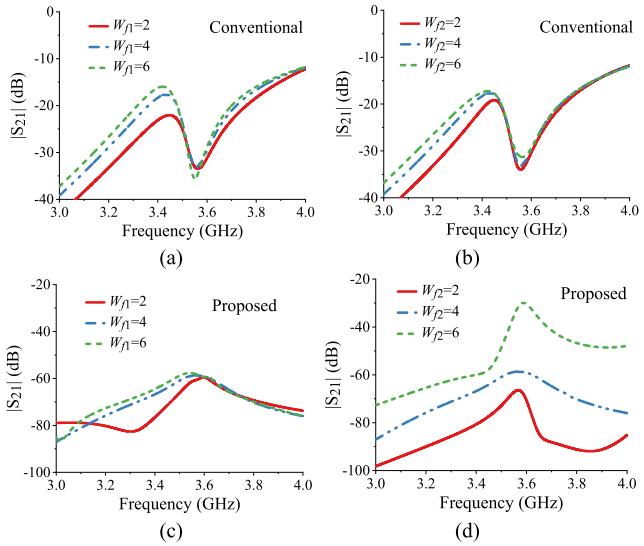

Fig. 8. Simulated isolations of the conventional and proposed duplex slot antenna versus the varying widths of the feeding slots. (a) W_{f1} for conventional one. (b) W_{f2} for conventional one. (c) W_{f1} for the proposed one. (d) W_{f2} for the proposed one. Dimensional unit: mm.

one of 58 dB. According to the previous analysis, it can be predicted that the isolation of conventional duplex antenna is affected by the sizes of both feeding slots 1 and 2, whereas the isolation of the proposed one is mainly affected by the sizes of feeding slot 2. To prove this, the effect of the widths of the feeding slots on the isolation of the two duplex antennas is shown in Fig. 8. Although both the increasing W_{f1} and W_{f2} cause a lower isolation of the conventional and proposed duplex antennas, for the conventional one, W_{f1} and W_{f2} have a similar effect on the isolation, whereas for the proposed one, W_{f2} has a much larger effect on the isolation than W_{f1}. These results verify the analysis in Figs. 5 and 6.

Even though the TE_{101} and TE_{011} modes have orthogonal electric field distributions with self-isolated performance, the isolation level still needs to be further discussed and designed. The highly improved isolation of the proposed IBFD antenna is realized by simply relocating the positions of the feeding structures without introducing other enhanced-isolation feeding structures.

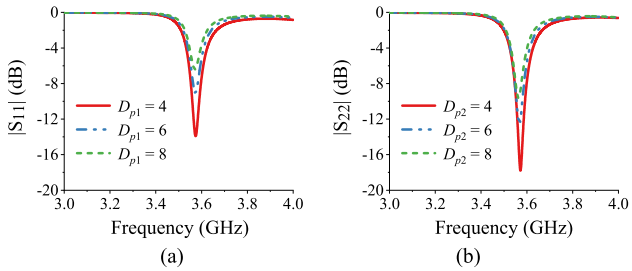

Fig. 9. Impedance matching. (a) Versus D_{p1} at port 1. (b) Versus D_{p2} at port 2. Dimensional unit: mm.

III. Designs of Narrowband IBFD Antennas

A. Narrowband Antenna

Section II has presented the basic design principle of the IBFD antenna, including the achievement of the same operating frequency and the analysis of the improved isolation. Then, the proposed design concept is used to design the IBFD slot antenna. We first present a duplex antenna based on the antenna structure in Fig. 1 with two crossed slots and the cavity modes TE_{101} and TE_{011}. Another mainly concerned performance for a practical antenna is the impedance matching. In fact, all the parameters can be used to achieve the impedance matching. For instance, Fig. 4 shows that the length of the feeding slot and radiation slot affects the frequencies as well as the impedance matching. The feeding slot affects the input impedance, and the radiation slot affects the radiation impedance. Therein, the length of the feeding slot has a little effect on the frequency, but it has a large effect on the impedance matching. Another main dimension to make the impedance matching is the distance between the probe and the feeding slot, i.e., D_{p1} and D_{p2}, as shown in Fig. 1. From Fig. 9, it can be seen that small distances D_{p1} and D_{p2} can achieve a better impedance matching and have a very little effect on the frequency shift.

Fig. 10 shows the simulated results of the IBFD antenna with crossed radiation slots shown in Fig. 1. It can be seen that this antenna operates at 3.54 GHz with a bandwidth of 0.8% ($|S_{11}| < -10$ dB). The realized gains of ports 1 and 2 are 6.2 and 6.4 dBi, respectively. Their total efficiencies are about 98%. Besides, the isolation is higher than 67 dB, which is achieved under the condition that the feeding slots and radiation slots of both channels are set in a single resonant cavity. In addition, the performance of the two channels, except for the isolation, can be individually optimized in such a configuration.

B. Narrowband Antenna With Enhanced Gain

To improve the radiation gain, the crossed radiation slots (Called Type-I) are replaced by two pairs of parallel slots (called Type-II), as shown in Fig. 11. Each channel has two parallel radiation slots for radiating the energy, which can consequently improve the radiation gain without enlarging the aperture size of the resonant cavity. Slot-1a and slot-1b only affect channel 1, whereas slot-2a and slot-2b only affect channel 2. Thus, the analysis and design procedures of

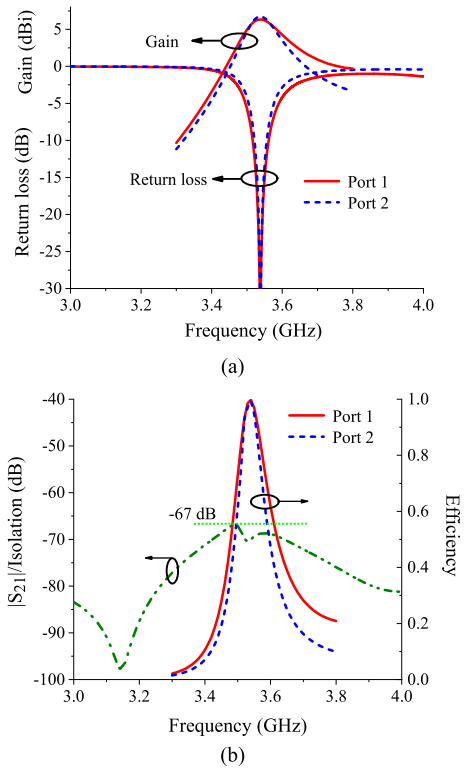

Fig. 10. Simulated results of the IBFD antenna with crossed slots. (a) Reflection coefficient and realized gain. (b) Isolation and efficiency. Dimensions (unit: mm): $a = 64$, $b = 66$, $c = 51$, $p_1 = 43$, $p_2 = 44$, $q_1 = q_2 = 30$, $s_1 = s_2 = 25$, $L_1 = 34.2$, $L_2 = 33$, $W_1 = W_2 = 8$, $L_{f1} = 34$, $L_{f2} = 36$, $W_{f1} = 6$, $W_{f2} = 3$, $L_{p1} = L_{p2} = 16$, $D_{p1} = 8$, $D_{p2} = 6$, $t_1 = t_2 = 3$, and $t_3 = 2$.

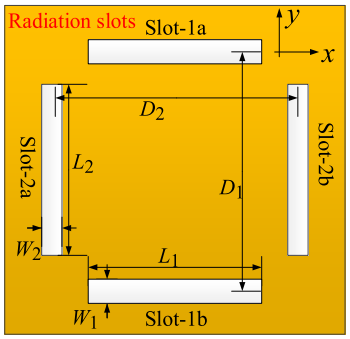

Fig. 11. View of the radiation slots of the duplex antenna with enhanced gain.

this antenna are similar to those of the antenna with crossed radiation slots. Here, the main difference between these two antennas is set as the distance between the parallel slots for discussion. In this context, the effect of D_1 on channel 1 is taken as an example, as shown in Fig. 12. It can be seen that a larger distance introduces a lower frequency and a higher radiation gain.

After the analysis and optimization, the simulated result of the IBFD antenna with an enhanced gain is shown in Fig. 13. It can be seen that this antenna operates at 3.52 GHz with a bandwidth of 0.8% ($|S_{11}| < -10$ dB), the isolation is higher than 64 dB, and the total efficiencies are about 98%. Fig. 13(b)

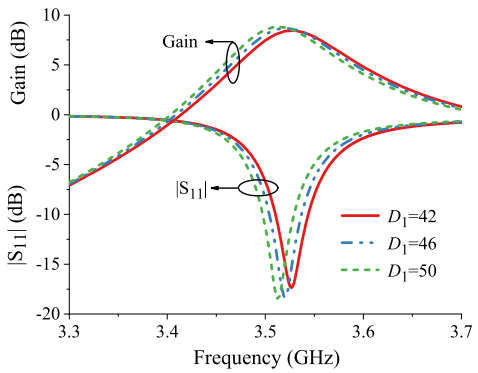

Fig. 12. Effect of D_1 on the operating frequency and realized gain of channel 1. Dimensional unit: mm.

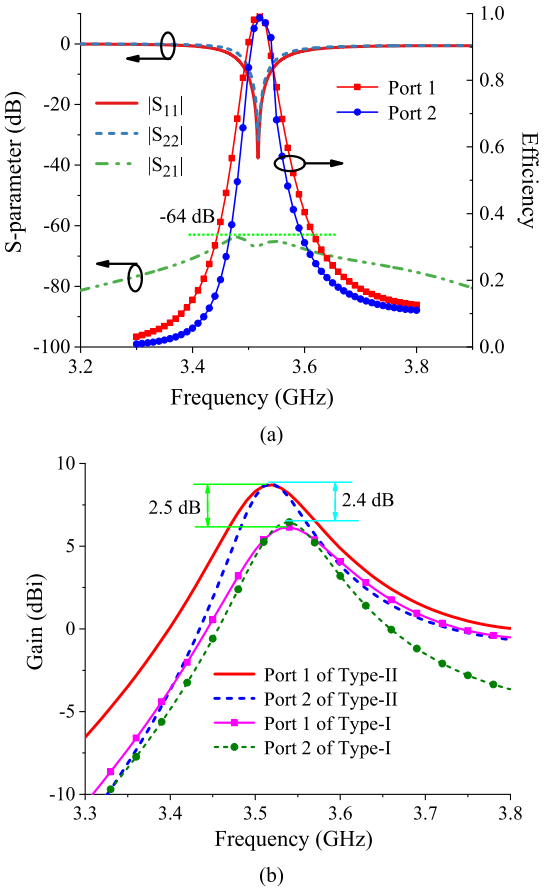

Fig. 13. Simulated results of the IBFD antenna with enhanced gain. (a) Reflection coefficient, isolation and efficiency. (b) Comparison of realized gain of Type-I and Type-II antennas. Dimensions (unit: mm): $a = 64$, $b = 66$, $c = 50$, $p_1 = 43$, $p_2 = 44$, $q_1 = q_2 = 30$, $s_1 = s_2 = 25$, $L_1 = 34$, $L_2 = 32.1$, $W_1 = 5$, $W_2 = 6$, $D_1 = 46$, $D_2 = 48$, $L_{f1} = 34$, $L_{f2} = 36$, $W_{f1} = 6$, $W_{f2} = 3$, $L_{p1} = 15.3$, $L_{p2} = 17$, $D_{p1} = 7$, $D_{p2} = 5$, $t_1 = t_2 = 3$, and $t_3 = 2$.

shows the comparison in the realized gains between the two types of antennas. Type-II antenna has 2.4–2.5-dB higher gain than Type-I antenna, which is about 8.7 and 8.8 dBi of ports 1 and 2, respectively, while their overall sizes are almost the same.

IV. Design of Wideband IBFD Antenna

The IBFD antennas presented previously show good performance with high isolation and easy design while

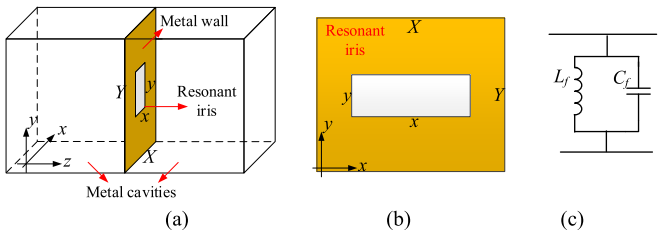

Fig. 14. Resonant iris. (a) Full view in a cavity. (b) Side view on a metal wall. (c) Equivalent circuit model.

suffering from narrow operating bandwidth, which causes a limited application. To obtain a wide operating bandwidth, the resonant-iris mode [27] is further excited and combined with the cavity mode to design the wideband IBFD antenna. The standard physical structure and equivalent circuit model of the resonant iris are shown in Fig. 14. The resonant iris is referred to as a slot on a metal wall, and this slotted wall is embedded into a metal cavity. The resonant iris can be equivalently regarded as a parallel *LC*-resonator, and the resonant frequency is calculated as follows [27]:

$$f_{iris} = \frac{v}{2}\sqrt{\frac{(Y^2 - y^2)}{(x^2Y^2 - X^2y^2)}}. \tag{3}$$

The configuration of the wideband IBFD antenna with two pairs of parallel radiation slots is shown in Fig. 15(a). Here, the feeding slots are used to obtain the resonant-iris modes, and the views and marked dimensions of them can be referred to Fig. 1(b) and (c). Based on (3), the resonant frequencies of these two resonant-iris modes are calculated as follows:

$$f_{s1} = \frac{v}{2}\sqrt{\frac{(b^2 - W_{f1}^2)}{(b^2L_{f1}^2 - a^2W_{f1}^2)}} \tag{4}$$

$$f_{s2} = \frac{v}{2}\sqrt{\frac{(a^2 - W_{f2}^2)}{(a^2L_{f2}^2 - c^2W_{f2}^2)}}. \tag{5}$$

The feeding slot in the proposed antenna can always produce a resonant-iris mode. However, in the previous designs, the resonant-iris mode produced by the feeding slot is not utilized, and it is purposively moved to higher frequency. This mode should be moved to lower frequency if it is used to design the dual-mode wideband antenna. According to (4) and (5), the lengths of the feeding slots have the largest effect on the resonant frequency. Thus, by properly increasing the lengths of the feeding slots, the resonant-iris modes will be shifted to lower frequency. As shown in Fig. 15(b), two resonant modes in each channel can be used to form a wide operating band. To clearly understand the resonant modes, the electric field distributions at these four frequencies are shown in Fig. 16. It can be seen that the lower resonant modes, i.e., f_1 and f_2, are the TE_{101} and TE_{011} modes of channels 1 and 2, respectively, whereas f_{s1} and f_{s2} are the resonant-iris modes related to feeding slots 1 and 2, respectively. Besides, the high isolation (higher than 63 dB) between the two channels is almost remained due to the orthogonal

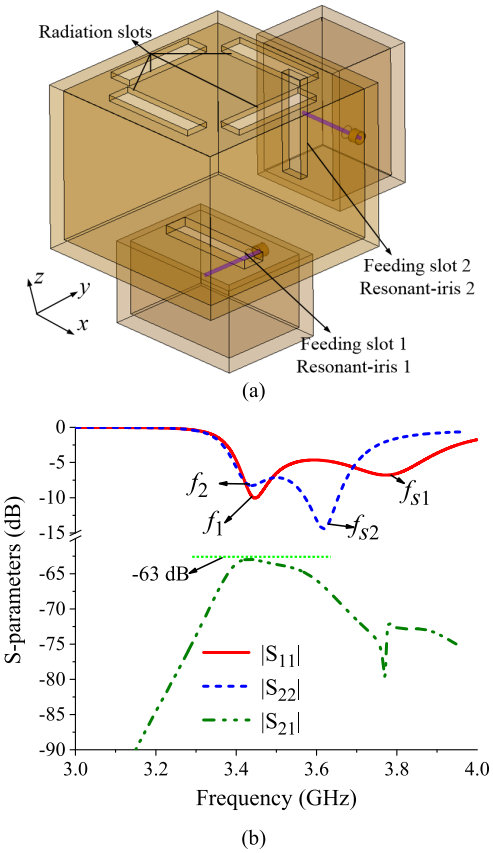

Fig. 15. (a) Configuration of the proposed wideband IBFD antenna with two pairs of parallel slots. (b) Initial performance of the wideband IBFD antenna. Dimensions (unit: mm): $a = 62$, $b = 60$, $c = 46$, $p_1 = p_2 = 43$, $q_1 = q_2 = 30$, $s_1 = s_2 = 25$, $L_1 = 37$, $L_2 = 38$, $W_1 = W_2 = 8$, $L_{f1} = 40$, $L_{f2} = 42$, $W_{f1} = 2$, $W_{f2} = 5$, $L_{p1} = 15$, $L_{p2} = 13$, $D_{p1} = 10$, $D_{p2} = 6$, $t_1 = 5$, $t_2 = 3$, and $t_3 = 3$.

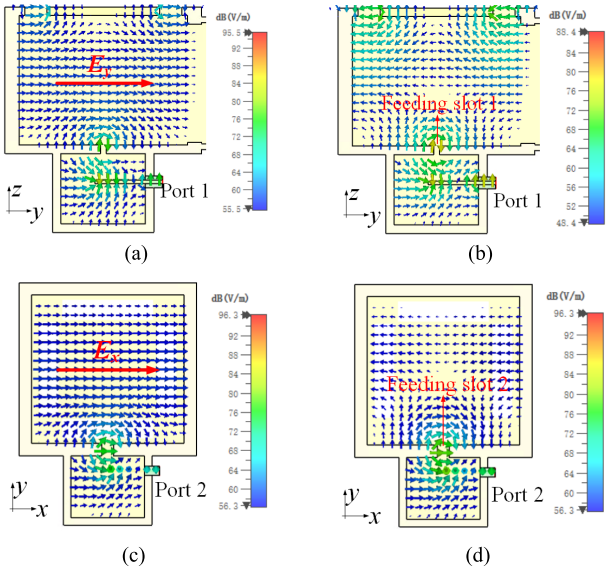

Fig. 16. Electric field distributions. (a) TE_{101} mode, f_1. (b) Resonant-iris mode of feeding slot 1, f_{s1}. (c) TE_{011} mode, f_2. (d) Resonant-iris mode of feeding slot 2, f_{s2}.

field distributions of both the cavity modes and resonant-iris modes, and the proposed arrangement of the feeding structure is shown in Fig. 1.

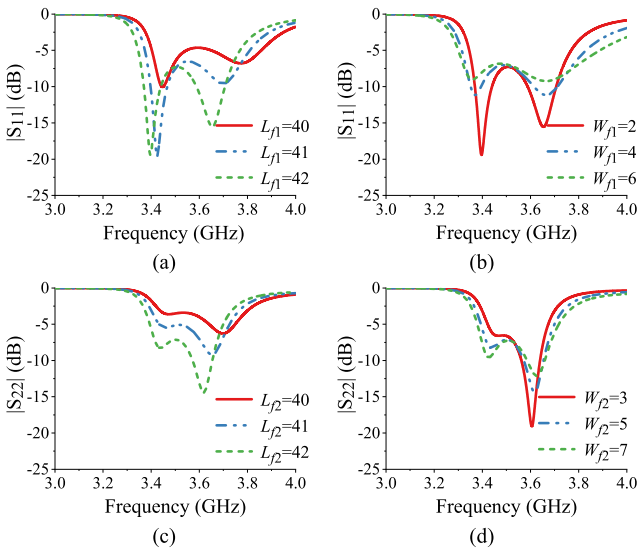

Fig. 17. Effect of the sizes of the feeding slots on the cavity modes and resonant-iris modes. (a) L_{f1} on channel 1. (b) W_{f1} on channel 1. (c) L_{f2} on channel 2. (b) W_{f2} on channel 2. Dimensional unit: mm.

TABLE I

COMPARISON OF THE CALCULATED AND SIMULATED FREQUENCIES OF RESONANT-IRIS MODES

a (mm)	b (mm)	L_{f1} (mm)	W_{f1} (mm)	Cal. f_{s1} (GHz)	Sim. f_{s1} (GHz)	Error
62	60	40	2	3.81	3.787	0.6%
62	60	41	2	3.717	3.7	0.46%
62	60	42	2	3.625	3.653	0.77%
62	60	42	2	3.625	3.653	0.77%
62	60	42	4	3.635	3.66	0.69%
62	60	42	6	3.65	3.67	0.55%
a (mm)	c (mm)	L_{f2} (mm)	W_{f2} (mm)	Cal. f_{s2} (GHz)	Sim. f_{s2} (GHz)	Error
62	46	40	5	3.81	3.72	2.5%
62	46	41	5	3.717	3.654	1.7%
62	46	42	5	3.63	3.618	0.3%
62	46	42	3	3.626	3.607	0.53%
62	46	42	5	3.628	3.616	0.33%
62	46	42	7	3.631	3.628	0.1%

On the one hand, from (3) to (5), it can be derived that a longer slot's length introduces a lower frequency of resonant-iris mode, whereas a wider slot's width introduces a higher frequency of resonant-iris mode. On the other hand, both longer slot's length and wider slot's width introduce a lower frequency of TE_{101}/TE_{011} cavity mode, as discussed in Section II. Thus, the effect of varying width can be used to justify the resonant-iris mode. To prove this analysis, the effect of the slots' sizes on the resonant modes is shown in Fig. 17. It can be seen that the tendency of the resonant frequencies of the cavity modes and resonant-iris modes affected by the slots' size is kept with the previous analysis. Besides, the length of the slot has a larger effect on the frequencies than the width, which is also kept with the derivation from (3) to (5). The comparison between the simulated and calculated resonant frequencies of the resonant-iris modes with varying slots' sizes is shown in Table I. It can be seen that the error between the simulated one and the calculated one is less than 2.5%.

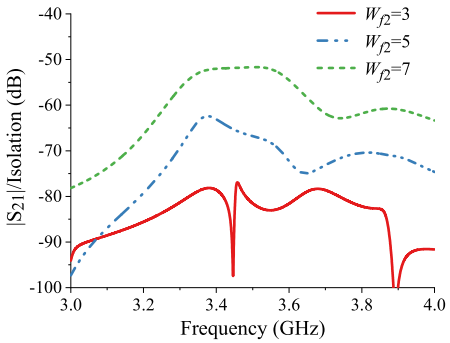

Fig. 18. Adjustment of isolation versus W_{f2}. Dimensional unit: mm.

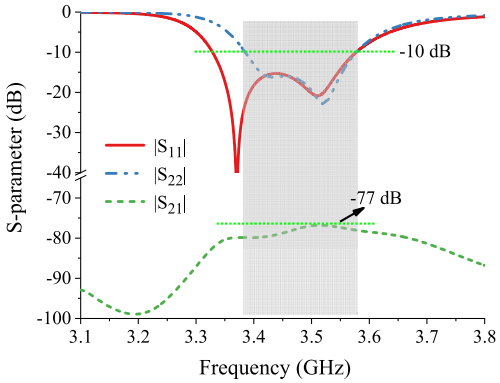

Fig. 19. Final simulated S-parameters of the wideband IBFD antenna. Dimensions (unit: mm): $a = 62$, $b = 60$, $c = 46$, $p_1 = 43$, $p_2 = 44$, $q_1 = q_2 = 30$, $s_1 = s_2 = 25$, $L_1 = 38$, $L_2 = 38$, $W_1 = 8$, $W_2 = 8$, $D_1 = 48$, $D_2 = 48$, $L_{f1} = 43$, $L_{f2} = 43$, $W_{f1} = 2$, $W_{f2} = 3$, $L_{p1} = 15.5$, $L_{p2} = 14$, $D_{p1} = 7$, $D_{p2} = 7$, $t_1 = 6$, $t_2 = 5$, and $t_3 = 2$.

The isolation of the wideband antenna is similar to that of the narrowband antenna presented in Sections III-A and III-B. Here, the main influenced factor, i.e., the width W_{f2}, is taken into the analysis, as shown in Fig. 18. It can be seen that a smaller W_{f2} can obtain a higher isolation.

Then, the antenna is designed and optimized with the simulated results, as shown in Fig. 19. The overlapping bandwidth with $|S_{11}| < -10$ dB of the two ports is from 3.383 to 3.578 GHz (195 MHz bandwidth, about 5.7%), and the isolation is higher than 77 dB over the operating band. Compared with the conventional design method, high isolation, enhanced gain, and enhanced bandwidth are achieved without introducing extra structure, enlarging cavity size, and deteriorating other antenna's performances.

V. EXPERIMENTAL RESULTS

The proposed wideband full-metal IBFD slot antenna is in the final fabricated and measured to validate the design concept. The antenna is fabricated using silver-plated brass to avoid oxidization and reduce the conductor loss. The photograph of the fabricated antenna is shown in Fig. 20. The antenna is fed by the SMA port with extended probe.

The simulated and measured S-parameters are shown in Fig. 21. The measured overlapping bandwidth is from 3.37 to 3.57 GHz (200 MHz bandwidth, about 5.8%), and

TABLE II
COMPARISONS WITH THE REPORTED IBFD ANTENNAS

Ref.	Freq. (GHz)	OBW	Structure	Technique for isolation	Isolation (dB)	Peak Gain (dBi)	TE	AE*	Aperture size ($\lambda_g \times \lambda_g$)
[1]	0.82	NA	PIFA	Dual antennas, Duplex filters Single-balanced feed	~30	NA	> 70%	NA	0.15×0.3
[6]	2.44	3.3%	Patch	Dual polarization Strip-loaded feed line	> 30	7.8	90%	NG	NG
[9]	5.69	19.3%	Patch	Dual polarization Single-balanced feed	> 57	14.3/13.2	> 90%.	74%/57%	3×1
[11]	2.45	3.4%	Patch	Dual polarization Single-balanced feed	> 50	5	~80%	34%	0.86×0.86
[13]	2.4	2.1%	Patch	Dual polarization Double-balanced feed	> 72	> 4	> 54%	NA	NG
[23]	10	19%$	SIW CBSA	Dual polarization Double-balanced feed	> 28	5.3	NG	51.3%	0.72×0.72
[24]	8.8	2.1%	SIW CBSA	Dual polarization Double-balanced feed	> 60	7.4	> 90%	33%	1.15×1.15
[25]	62	5%^	Full-metal CBSA	Dual polarization Multilayer feeding network	> 52	32.3	NG	>70%	12.9×12.9
[26]	13.6	17.1%	Full-metal CBSA	Dual polarization Multilayer feeding network	> 40	31.4	NG	>70%	11.37×11.37
This work	3.47	5.8%	Full-metal CBSA	Dual polarization Modified orthogonal feeding structure	> 72	8.8	> 95%	> 80%	0.78×0.76+0.4×0.32#

OBW: Overlapping bandwidth of two ports with $|S_{11}| < -10$ dB. TE: Total efficiency; AE: Aperture efficiency; NG: Not given; NA: Not applicable.
*The aperture efficiency is not provided directly by the authors, it is calculated according to the realized gain and physical aperture size.
$Bandwidth with VSWR<2.1 ($|S_{11}| < -9$ dB); ^Simulated bandwidth, the measured results was deteriorated, which is not given;
#Include the size of the top wall of the feeding cavity 2. All the physical aperture size contributes to the realized gain, not only the aperture size that the radiating elements cover.

Fig. 20. Photograph of the proposed wideband IBFD slot antenna.

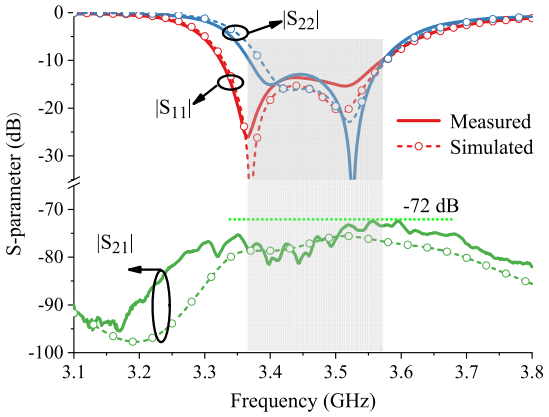

Fig. 21. Measured and simulated S-parameters of the proposed antenna.

the in-band isolation is higher than 72 dB, which is a little lower than the simulated one of 77 dB. The proposed cavity-backed IBFD slot antenna has a higher isolation than the

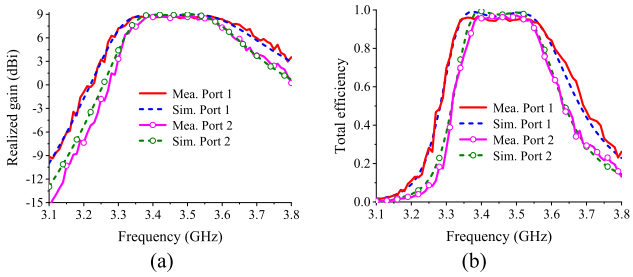

Fig. 22. Measured and simulated results. (a) Realized gain. (b) Total efficiency.

reported IBFD CBSAs [23]–[26]. The measured realized gains of the two ports are higher than 8.5 dBi with a peak gain of 8.8 dBi, whereas the simulated ones are higher than 8.7 dBi with a peak gain 9 dBi, as shown in Fig. 22(a). The measured total efficiencies are higher than 94% with a peak efficiency of 97%, whereas the simulated ones are higher than 97% with a peak efficiency of 99%, as shown in Fig. 22(b). The radiation patterns shown in Fig. 23 indicate that the measured coplanar polarizations (co-pol) of the two ports are almost the same as the simulated ones. Besides, the measured cross-polarizations (X-pol) of the two ports at *XZ* plane are better than 30 dB, whereas the X-pols are better than 23 dB at *YZ* plane.

The comparison with other reported IBFD antennas is shown in Table II. It can be seen that the proposed antenna has the highest isolation, especially compared with the IBFD CBSA. The work [13] has the same isolation, while two

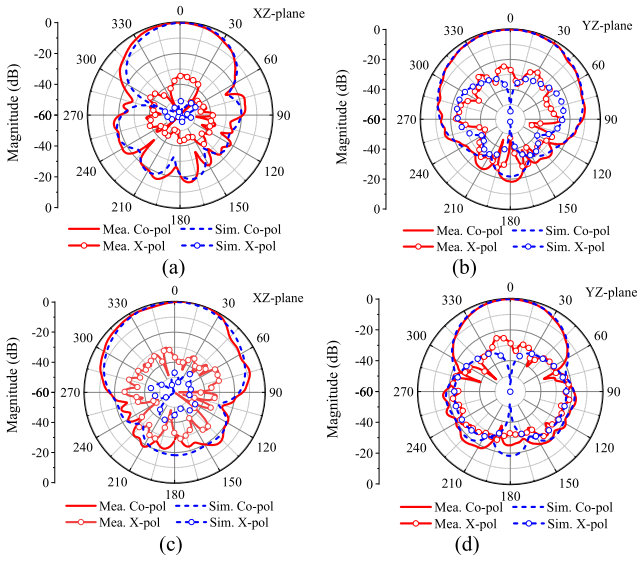

Fig. 23. Measured and simulated radiation patterns at 3.5 GHz. (a) Port 1 at *XZ* plane. (b) Port 1 at *YZ* plane. (c) Port 2 at *XZ* plane. (d) Port 2 at *YZ* plane.

extra 3 dB/180° couplers were used to feed the patch antenna to obtain a high isolation. Besides, the proposed antenna also owns the merits of high total efficiency and high aperture efficiency. In addition, the full-metal structure brings out a high-power-handling capacity.

VI. Conclusion

High-isolation IBFD CBSAs in a single-metal resonant cavity are presented in this article. The proposed arrangement of the feeding structures can obtain a much higher isolation than conventional one. An enhanced gain is obtained by replacing the crossed slots with two pairs of parallel slots. Besides, the resonant-iris modes produced by the feeding slots are combined with the cavity modes to obtain an enhanced operating bandwidth. The achievements of the improved isolation, enhanced gain, and enhanced bandwidth are obtained without introducing any other antenna structure. The final measured prototype shows that the proposed full-metal IBFD CBSA has a 5.8% bandwidth, a 95% total efficiency, and an 80% aperture efficiency for both two channels. Especially, the isolation between the two channels is higher than 72 dB over the operating band.

References

[1] O. N. Alrabadi, A. D. Tatomirescu, M. B. Knudsen, M. Pelosi, and G. F. Pedersen, "Breaking the transmitter–receiver isolation barrier in mobile handsets with spatial duplexing," *IEEE Trans. Antennas Propag.*, vol. 61, no. 4, pp. 2241–2251, Apr. 2013.

[2] T. Dinc and H. Krishnaswamy, "A T/R antenna pair with polarization-based reconfigurable wideband self-interference cancellation for simultaneous transmit and receive," in *IEEE MTT-S Int. Microw. Symp. Dig.*, Phoenix, AZ, USA, May 2015, pp. 1–4.

[3] X. Wang, W. Che, W. Yang, W. Feng, and L. Gu, "Self-interference cancellation antenna using auxiliary port reflection for full-duplex application," *IEEE Antennas Wireless Propag. Lett.*, vol. 16, pp. 2873–2876, 2017.

[4] J. Wu, M. Li, and N. Behdad, "A wideband, unidirectional circularly polarized antenna for full-duplex applications," *IEEE Trans. Antennas Propag.*, vol. 66, no. 3, pp. 1559–1563, Mar. 2018.

[5] S. Khaledian, F. Farzami, B. Smida, and D. Erricolo, "Inherent self-interference cancellation for in-band full-duplex single-antenna systems," *IEEE Trans. Microw. Theory Techn.*, vol. 66, no. 6, pp. 2842–2850, Jun. 2018.

[6] C. X. Mao, Y. Zhou, Y. Wu, H. Soewardiman, D. H. Werner, and J. S. Jur, "Low-profile strip-loaded textile antenna with enhanced bandwidth and isolation for full-duplex wearable applications," *IEEE Trans. Antennas Propag.*, vol. 68, no. 9, pp. 6527–6537, Sep. 2020.

[7] H. Nawaz and I. Tekin, "Dual port single patch antenna with high interport isolation for 2.4 GHz in-band full duplex wireless applications," *Microw. Opt. Technol. Lett.*, vol. 58, no. 7, pp. 1756–1759, Jul. 2016.

[8] C.-Y.-D. Sim, C.-C. Chang, and J.-S. Row, "Dual-feed dual-polarized patch antenna with low cross polarization and high isolation," *IEEE Trans. Antennas Propag.*, vol. 57, no. 10, pp. 3321–3324, Oct. 2009.

[9] D. Wójcik, M. Surma, A. Noga, and M. Magnuski, "High port-to-port isolation dual-polarized antenna array dedicated for full duplex base stations," *IEEE Antennas Wireless Propag. Lett.*, vol. 14, no. 8, pp. 1–5, Aug. 2015.

[10] G. Makar, N. Tran, and T. Karacolak, "A high-isolation monopole array with ring hybrid feeding structure for in-band full-duplex systems," *IEEE Antennas Wireless Propag. Lett.*, vol. 16, pp. 356–359, 2017.

[11] C. Goodbody, T. Karacolak, and N. Tran, "Dual-polarised patch antenna for in-band full-duplex applications," *Electron. Lett.*, vol. 54, no. 22, pp. 1255–1256, Nov. 2018.

[12] H. Nawaz and I. Tekin, "Compact dual-polarised microstrip patch antenna with high interport isolation for 2.5 GHz in-band full-duplex wireless applications," *IET Microw., Antennas Propag.*, vol. 11, no. 7, pp. 976–981, Jun. 2017.

[13] H. Nawaz and I. Tekin, "Double-differential-fed, dual-polarized patch antenna with 90 dB interport RF isolation for a 2.4 GHz in-band full-duplex transceiver," *IEEE Antennas Wireless Propag. Lett.*, vol. 17, no. 2, pp. 287–290, Feb. 2018.

[14] M. Yilan, H. Ayar, H. Nawaz, O. Gurbuz, and I. Tekin, "Monostatic antenna in-band full duplex radio: Performance limits and characterization," *IEEE Trans. Veh. Technol.*, vol. 68, no. 5, pp. 4786–4799, May 2019.

[15] Z. Zhang, X. Cao, J. Gao, S. Li, and J. Han, "Broadband SIW cavity-backed slot antenna for endfire applications," *IEEE Antennas Wireless Propag. Lett.*, vol. 17, no. 7, pp. 1271–1275, Jul. 2018.

[16] S. Liao, P. Chen, P. Wu, K. M. Shum, and Q. Xue, "Substrate-integrated waveguide-based 60-GHz resonant slotted waveguide arrays with wide impedance bandwidth and high gain," *IEEE Trans. Antennas Propag.*, vol. 63, no. 7, pp. 2922–2931, Jul. 2015.

[17] D.-F. Guan, Z.-P. Qian, Y.-S. Zhang, and Y. Cai, "Novel SIW cavity-backed antenna array without using individual feeding network," *IEEE Antennas Wireless Propag. Lett.*, vol. 13, pp. 423–426, 2014.

[18] W. Li, K. D. Xu, X. Tang, Y. Yang, Y. Liu, and Q. H. Liu, "Substrate integrated waveguide cavity-backed slot array antenna using high-order radiation modes for dual-band applications in *K*-band," *IEEE Trans. Antennas Propag.*, vol. 65, no. 9, pp. 4556–4565, Sep. 2017.

[19] Y.-M. Wu, S.-W. Wong, J.-Y. Lin, L. Zhu, Y. He, and F.-C. Chen, "A circularly polarized cavity-backed slot antenna with enhanced radiation gain," *IEEE Antennas Wireless Propag. Lett.*, vol. 17, no. 6, pp. 1010–1014, Jun. 2018.

[20] J.-Y. Lin *et al.*, "A dual-functional triple-mode cavity resonator with the integration of filters and antennas," *IEEE Trans. Antennas Propag.*, vol. 66, no. 5, pp. 2589–2593, May 2018.

[21] Y.-M. Wu, S.-W. Wong, H. Wong, and F.-C. Chen, "A design of bandwidth-enhanced cavity-backed slot filtenna using resonance windows," *IEEE Trans. Antennas Propag.*, vol. 67, no. 3, pp. 1926–1930, Mar. 2019.

[22] W. Yuan, X. Liang, L. Zhang, J. Geng, W. Zhu, and R. Jin, "Rectangular grating waveguide slot array antenna for SATCOM applications," *IEEE Trans. Antennas Propag.*, vol. 67, no. 6, pp. 3869–3880, Jun. 2019.

[23] R. C. Paryani, P. F. Wahid, and N. Behdad, "A wideband, dual-polarized, substrate-integrated cavity-backed slot antenna," *IEEE Antennas Wireless Propag. Lett.*, vol. 9, pp. 645–648, 2010.

[24] G. Srivastava and A. Mohan, "A differential dual-polarized SIW cavity-backed slot antenna," *IEEE Trans. Antennas Propag.*, vol. 67, no. 5, pp. 3450–3454, May 2019.

[25] D. Kim, M. Zhang, J. Hirokawa, and M. Ando, "Design and fabrication of a dual-polarization waveguide slot array antenna with high isolation and high antenna efficiency for the 60 GHz band," *IEEE Trans. Antennas Propag.*, vol. 62, no. 6, pp. 3019–3027, Jun. 2014.

[26] S.-G. Zhou, G.-L. Huang, T.-H. Chio, J.-J. Yang, and G. Wei, "Design of a wideband dual-polarization full-corporate waveguide feed antenna array," *IEEE Trans. Antennas Propag.*, vol. 63, no. 11, pp. 4775–4782, Nov. 2015.
[27] T.-S. Chen, "Characteristics of waveguide resonant-iris filters (correspondence)," *IEEE Trans. Microw. Theory Techn.*, vol. MTT-15, no. 4, pp. 260–262, Apr. 1967.

Rui-Sen Chen (Graduate Student Member, IEEE) was born in Fujian, China. He received the B.S. degree from the Hunan University of Science and Technology, Xiangtan, Hunan, China, in 2012, and the master's degree in electromagnetic field and radio technology from the South China University of Technology, Guangzhou, China, in 2015. He is currently pursuing the Ph.D. degree with the College of Electronics and Information Engineering, Shenzhen University, Shenzhen, China.

He is currently a Research Assistant with the Faculty of Science and Technology, University of Macau, Macau, China. His current research interests include microwave filters and antenna and cavity components.

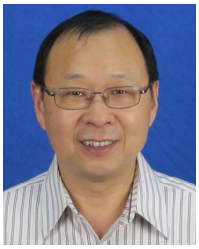

Lei Zhu (Fellow, IEEE) received the B.Eng. and M.Eng. degrees in radio engineering from the Nanjing Institute of Technology (now Southeast University), Nanjing, China, in 1985 and 1988, respectively, and the Ph.D. degree in electronic engineering from The University of Electro-Communications, Tokyo, Japan, in 1993.

From 1993 to 1996, he was a Research Engineer with Matsushita-Kotobuki Electronics Industries Ltd., Tokyo. From 1996 to 2000, he was a Research Fellow with the École Polytechnique de Montreal, Montreal, QC, Canada. From 2000 to 2013, he was an Associate Professor with the School of Electrical and Electronic Engineering, Nanyang Technological University, Singapore. In August 2013, he joined the Faculty of Science and Technology, University of Macau, Macau, China, as a Full Professor, where he has been a Distinguished Professor since December 2016. From August 2014 to August 2017, he was the Head of the Department of Electrical and Computer Engineering, University of Macau. So far, he has authored or coauthored more than 580 papers in international journals and conference proceedings. His papers have been cited more than 10 000 times with an H-index of 51 (source: Scopus). His research interests include microwave circuits, planar antennas, periodic structures, and computational electromagnetics.

Dr. Zhu served as a member for the IEEE MTT-S Fellow Evaluation Committee from 2013 to 2015 and the IEEE AP-S Fellows Committee from 2015 to 2017. He was a recipient of the 1997 Asia–Pacific Microwave Prize Award, the 1996 Silver Award of Excellent Invention from Matsushita-Kotobuki Electronics Industries Ltd., and the 1993 First-Order Achievement Award in Science and Technology from the National Education Committee, China. He served as the General Chair for the 2008 IEEE MTT-S International Microwave Workshop Series on the Art of Miniaturizing RF and Microwave Passive Components, Chengdu, China, and the Technical Program Committee Co-Chair for the 2009 Asia–Pacific Microwave Conference, Singapore. He was an Associate Editor of the IEEE TRANSACTIONS ON MICROWAVE THEORY AND TECHNIQUES from 2010 to 2013 and IEEE MICROWAVE AND WIRELESS COMPONENTS LETTERS from 2006 to 2012.

Jing-Yu Lin (Graduate Student Member, IEEE) received the B.E. degree from Southwest Jiaotong University (SWJTU), Chengdu, China, in 2016, and the M.E. degree from the School of Electronic and Information Engineering, South China University of Technology (SCUT), Guangzhou, China, in 2018. He is currently pursuing the Ph.D. degree with the University of Technology Sydney (UTS), Ultimo, NSW, Australia.

From October 2017 to February 2019, he was as an Exchange Student with the University of Technology Sydney. His current research interest includes microwave cavity circuit design.

Sai-Wai Wong (Senior Member, IEEE) received the B.S degree in electronic engineering from The Hong Kong University of Science and Technology, Hong Kong, in 2003, and the M.Sc. and Ph.D. degrees in communication engineering from Nanyang Technological University, Singapore, in 2006 and 2009, respectively.

From July 2003 to July 2005, he was an Electronic Engineer to lead the Electronic Engineering Department in China with two Hong Kong manufacturing companies. From May 2009 to October 2010, he was a Research Fellow with the ASTAR Institute for Infocomm Research, Singapore. Since 2010, he has been an Associate Professor and later become a Full Professor at the School of Electronic and Information Engineering, South China University of Technology, Guangzhou, China. From July 2016 to September 2016, he was a Visiting Professor with the City University of Hong Kong, Hong Kong. Since 2017, he has been a Full Professor with the College of Electronics and Information Engineering, Shenzhen University, Shenzhen, China. So far, he has authored or coauthored more than 200 papers in international journals and conference proceedings. His current research interests include RF/microwave circuit and antenna design.

Dr. Wong was a recipient of the New Century Excellent Talents in University by the Ministry of Education of China in 2013 and the Shenzhen Overseas High-Caliber Personnel Level C in 2018.

Yang Yang (Senior Member, IEEE) was born in Bayannur, Inner Mongolia, China. He received the Ph.D. degree from the Department of Electrical and Computer Systems Engineering, Monash University, Melbourne, VIC, Australia, in 2013.

He has three years of industry experience at Rain Bird Australia, Deer Park, VIC, Australia, as an Asia–Pacific GSP Engineer, from 2012 to 2015. In April 2015, he returned to academia and served as a Senior Research Associate with the Centre for Collaboration in Electromagnetic and Antenna Engineering, Macquarie University, Sydney, NSW, Australia. In April 2016, he was appointed as a Research Fellow at the State Key Laboratory of Terahertz and Millimeter Waves, City University of Hong Kong, Hong Kong. Since December 2016, he has been with the University of Technology Sydney, Sydney. He is currently a Senior Lecturer and a Team Leader of millimeter-wave integrated circuits and antennas. He has over 150 international peer-reviewed publications in microwave and millimeter-wave circuits and antennas. His research interests include millimeter-wave and subterahertz technologies in 5G and biomedical applications.

Dr. Yang is a Committee Member of the MTT-28 Biological Effects and Medical Applications. He received the CST University Publication Award 2018, by CST, Dassault Systèmes, and the corporate 2014 Global GSP Success Award (one globally). He is also an Associate Editor of IEEE ACCESS and an Area Editor of *Microwave and Optical Technology Letters*.

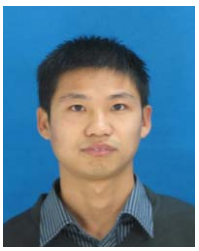

Yin Li (Member, IEEE) received the B.S. degree in applied physics from the China University of Petroleum, Dongying, China, in 2009, the M.Eng. degree in electromagnetic field and microwave technology from the University of Electronic Science and Technology of China (UESTC), Chengdu, China, in 2012, and the Ph.D. degree from the University of Macau, Macau, China, in 2018.

From 2013 to 2015, he was a Research Assistant with The University of Hong Kong (HKU), Hong Kong. He is currently a Post-Doctoral Fellow with the School of Electronics and Information, Shenzhen University, Shenzhen, China. His current research interests include numerical modeling methods of passive microwave circuits, computational electromagnetics, and microwave circuits, frequency selectivity surface, and filtering antennas.

Long Zhang (Member, IEEE) received the B.S. and M.S. degrees in electrical engineering from the Huazhong University of Science and Technology (HUST), Wuhan, China, in 2009 and 2012, respectively, and the Ph.D. degree in electronic engineering from the University of Kent, Canterbury, U.K, in 2017.

He was a Research Fellow with the Poly-Grames Research Center, Polytechnique Montreal, Montreal, QC, Canada. He is currently an Assistant Professor with the College of Electronics and Information Engineering, Shenzhen University, Shenzhen, China. His current research interests include circularly polarized antennas and arrays, millimeter-wave antennas and arrays, tightly coupled arrays, reflectarrays, and characteristics mode theory.

Dr. Zhang served as a Reviewer for several technique journals, including the IEEE TRANSACTIONS ON ANTENNAS AND PROPAGATION, the IEEE ANTENNAS AND WIRELESS PROPAGATION LETTERS, the *IET Microwaves, Antennas & Propagation*, and the *Electronic Letters*.

Yejun He (Senior Member, IEEE) received the Ph.D. degree in information and communication engineering from the Huazhong University of Science and Technology (HUST), Wuhan, China, in 2005.

He has been a Full Professor with the College of Electronics and Information Engineering, Shenzhen University, Shenzhen, China, where he is currently the Director of the Guangdong Engineering Research Center of Base Station Antennas and Propagation and the Director of the Shenzhen Key Laboratory of Antennas and Propagation. He was selected as a Pengcheng Scholar Distinguished Professor, Shenzhen, China. He has authored or coauthored more than 180 research articles and books (chapters). He holds about 20 patents. His research interests include wireless communications, antennas, and radio frequency.

Dr. He is a fellow of IET and the Chair of the IEEE Antennas and Propagation Society-Shenzhen Chapter. He was a recipient of the Shenzhen Overseas High-Caliber Personnel Level B ("Peacock Plan Award" B) and Shenzhen High-Level Professional Talent (Local Leading Talent). He received the 2016 Shenzhen Science and Technology Progress Award and the 2017 Guangdong Provincial Science and Technology Progress Award. He served as the General Chair for IEEE ComComAp 2019. He is serving as an Associate Editor for *IEEE Network*, *International Journal of Communication Systems*, and *China Communications*.